Molecular Crystals and Liquid Crystals

ISSN: 1542-1406 (Print) 1563-5287 (Online) Journal homepage: http://www.tandfonline.com/loi/gmcl20

Crystal structure, spectroscopic properties, and DFT studies of 2-(2-hydroxyphenyl)benzo[d]oxazole-6-carbaldehyde

Kew-Yu Chen

To cite this article: Kew-Yu Chen (2016) Crystal structure, spectroscopic properties, and DFT studies of 2-(2-hydroxyphenyl)benzo[d]oxazole-6-carbaldehyde, Molecular Crystals and Liquid Crystals, 625:1, 212-220, DOI: 10.1080/15421406.2015.1069465

To link to this article: http://dx.doi.org/10.1080/15421406.2015.1069465

Published online: 19 Feb 2016.

MOL. CRYST. LIQ. CRYST.
2016, VOL. 625, 212–220
http://dx.doi.org/10.1080/15421406.2015.1069465

Taylor & Francis
Taylor & Francis Group

Crystal structure, spectroscopic properties, and DFT studies of 2-(2-hydroxyphenyl)benzo[d]oxazole-6-carbaldehyde

Kew-Yu Chen

Department of Chemical Engineering, Feng Chia University, Taichung, Taiwan, ROC

ABSTRACT

The title compound 2-(2-hydroxyphenyl)benzo[d]oxazole-6-carbaldehyde (**1a**) was synthesized and characterized by single-crystal X-ray diffraction. Compound **1a** possesses intramolecular C–H···O and O–H···N hydrogen bonds, which generate S(5) and S(6) rings, respectively. Intermolecular π–π stacking is observed in the crystal structure, which links a pair of molecules into a cyclic centrosymmetric dimer. The crystal structure is further stabilized by three different intermolecular C–H···O hydrogen bonds, which link the molecules into a continuous three-dimensional framework. Its spectroscopic properties and complementary density functional theory (DFT) calculations are also reported.

KEYWORDS

Benzothiazole derivatives; benzoxazole derivatives; DFT calculations; ESIPT; X-ray diffraction

1. Introduction

The excited-state intramolecular proton transfer (ESIPT) reaction of 2-(benzo[d]oxazol-2-yl)phenol and its derivatives has been investigated using the femtosecond fluorescence up-conversion technique [1]. The ESIPT reaction involves transfer of a phenolic hydroxyl proton to an imine nitrogen through an intramolecular six-membered-ring hydrogen-bonding configuration [2–6], as depicted in Fig. 1. The resulting proton-transfer tautomer (keto-form) shows great differences in structure and electronic configuration from its corresponding ground state, i.e., a large Stokes shifted $K^* \rightarrow K$ fluorescence. This unique photophysical property has found a number of important applications such as probes for solvation dynamics [7–9] and biological environments [10,11], chemosensors [12–16], fluorescence microscopy imaging [17], photochromic materials [18], nonlinear optical materials [19], near-infrared fluorescent dyes [20], and organic light-emitting devices [21–25]. To expand the scope of benzoxazole-based chromophores available for designing systems for highly fluorescent dyes and organic optoelectronic materials, the present research reports the synthesis of a 2-(benzo[d]oxazol-2-yl)phenol derivative 2-(2-hydroxyphenyl)benzo[d]oxazole-6-carbaldehyde (**1a**) as well as its X-ray structure, optical properties, and complementary density functional theory (DFT) calculations. The results offer the potential to synthesize 2-(benzo[d]oxazol-2-yl)phenol derivatives with extended molecular architectures and photophysical properties.

CONTACT Kew-Yu Chen kyuchen@fcu.edu.tw Department of Chemical Engineering, Feng Chia University, 40724 Taichung, Taiwan, ROC.

Color versions of one or more of the figures in the article can be found online at www.tandfonline.com/gmcl.

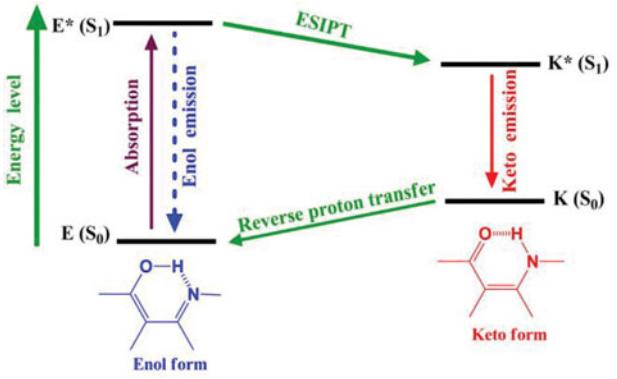

Figure 1. Characteristic four-level photocycle scheme of the ESIPT process.

2. Experimental

2.1. *Chemicals and instruments*

The starting materials such as 2-hydroxybenzaldehyde (**7**), 6-amino-m-cresol (**6a**), lead (IV) acetate, acetic acid, acetic anhydride, N-bromosuccinimide (NBS), azobisisobutyronitrile (AIBN), and hexamethylenetetramine (HMTA) were purchased from Merck, ACROS and Sigma-Aldrich. Column chromatography was performed using silica gel Merck Kieselgel si 60 (40–63 mesh).

^{1}H and ^{13}C NMR spectra were recorded in $CDCl_3$ on a Bruker 500 MHz. Mass spectra were recorded on a VG70-250S mass spectrometer. The absorption and emission spectra were measured using a Jasco V-570 UV-Vis spectrophotometer and a Hitachi F-7000 fluorescence spectrophotometer, respectively. The single-crystal X-ray diffraction data were collected on a Bruker Smart 1000CCD area-detector diffractometer.

2.2. *Synthesis and characterization*

2.2.1. *Synthesis of 1a*

Hexamethylenetetramine (HMTA) (1.2 g, 8.6 mmol) was added to a solution of **3a** (1.4 g, 4.1 mmol) in 50 mL of $CHCl_3$. The mixture was refluxed for 8 hr. After the mixture was cooled, the residual precipitate was filtered and dried. Next, to 10 mL of glacial acetic acid and 10 mL of water, dried salt was added and refluxed for 2 hr. After it was cooled, the mixture was neutralized with aqueous NaOH solution and was extracted with CH_2Cl_2. The organic layer was dried with anhydrous $MgSO_4$ and evaporated. The mixture of **1a** and **2a** was dissolved in a suspension of 0.3 g of KOH in 50 mL of CH_2Cl_2. The mixture was gently boiled for 4 hr. After it was cooled, the solution was poured into water and neutralized with aqueous HCl solution. The mixture was extracted with CH_2Cl_2 and dried with anhydrous $MgSO_4$. After the solvent was removed, the crude product was purified by silica gel column chromatography with eluent ethylacetate/n-hexane (1/4) to afford **1a**. ^{1}H NMR (500 MHz, $CDCl_3$, in ppm) δ 11.18 (s, 1H), 10.06 (s, 1H), 8.08 (s, 1H), 8.02 (d, J = 8.6 Hz, 1H), 7.91 (d, J = 8.3 Hz, 1H), 7.82 (d, J = 8.3 Hz, 1H), 7.48 (t, J = 7.6 Hz, 1H), 7.11 (d, J = 8.4 Hz, 1H), 7.02 (t, J = 7.6 Hz, 1H). ^{13}C NMR (125 MHz, $CDCl_3$, ppm): 190.69, 165.97, 159.21, 149.27, 145.16, 134.65, 133.90, 127.73, 127.51, 119.83, 119.45, 117.67, 111.19, 109.76. MS (EI, 70 eV): m/z (relative intensity) 239 (M^+, 100). HRMS calcd for $C_{14}H_9NO_3$, 239.0582; found, 239.0586. Yellow parallelepiped

crystals suitable for the crystallographic studies reported here were isolated over a period of 5 weeks by slow evaporation from a dichloromethane solution.

2.2.2. *Crystal structural determination*

A single crystal of the title compound with dimensions of 0.58 mm × 0.10 mm × 0.08 mm was selected. The lattice constants and diffraction intensities were measured with a Bruker Smart 1000CCD area detector radiation ($\lambda = 0.71073$ Å) at 110(2) K. An ω-2θ scan mode was used for data collection in the range of $3.19^{o} \leqq \theta \leqq 29.18^{o}$. A total of 4643 reflections were collected and 2430 were independent ($R_{int} = 0.0232$), of which 1664 were considered to be observed with $I > 2\sigma(I)$ and used in the succeeding refinement. The structure was solved by direct methods with SHELXS-97 [26] and refined on F^2 by full-matrix least-square procedure with Bruker SHELXL-97 packing [27]. All non-hydrogen atoms were refined with anisotropic thermal parameters. The hydrogen atoms refined with riding model position parameters isotropically were located from difference Fourier map and added theoretically. At the final cycle of refinement, $R = 0.0548$ and $wR = 0.1012$ ($w = 1/[\sigma^2(F_o^2) + (0.0465P)^2 + 0.0000P]$, where $P = (F_o^2 + 2F_c^2)/3$), $S = 1.000$, $(\Delta/\sigma)_{max} = 0.001$, $(\Delta/\rho)_{max} = 0.242$, and $(\Delta/\rho)_{min} = -0.262$ e Å^{-3}. Crystallographic data for compound **1a** have been deposited with the Cambridge Crystallographic Data Center as supplementary publication number CCDC 1044863. Copies of these information can be obtained free of charge from the Director, CCDC, 12 Union Road, Cambridge CB2 1EZ, UK (fax: +44 1223 336 033; E-mail: deposit@ccdc.cam.ac.uk).

2.3. *Computational methods*

The Gaussian 03 program was used to perform the ab initio calculation on the molecular structure [28]. Geometry optimization for compound **1a** was carried out with the 6-31G** basis set to the B3LYP functional. After obtaining the converged geometries, the TD-B3LYP/6-31G** was used to calculate the vertical excitation energy, and the emission energy was obtained from TDDFT/B3LYP/6-31G** calculations performed on S_1 optimized geometries.

3. Results and discussion

Scheme 1 shows the synthetic route and the chemical structures of **1a** and **1b**. In brief, the synthesis of **1a** started from a condensation of 2-hydroxybenzaldehyde (**7a**) and 6-amino-m-cresol (**6a**), followed by the acetylation of benzoxazol (**5a**), giving an ester compound **4a**. Next, the bromination of **4a** allowed for efficient synthesis of benzyl bromide (**3a**), followed by the oxidation of the bromo adduct to give an aldehyde compound **2a**. Finally, the protected hydroxyl group was deprotected by KOH to give **1a**. The presence of a single carbonyl substituent of **1a** can be verified by the presence of a signal at δ 10.06 ppm and seven signals at δ 6.9–8.1 ppm in the ^{1}H NMR spectrum. Detailed synthetic procedures and product characterization are provided in the Experimental section. To confirm its structure, a single crystal of **1a** was obtained from a dichloromethane solution, and the molecular structure was determined by X-ray diffraction analysis. Moreover, its X-ray structure is compared with that of **1b** [29].

Figure 2 shows the ORTEP diagram of **1a**. Compound **1a**, as well as compound **1b**, crystallizes in the monoclinic space group $P2_1/c$ (Table 1). The complete molecule of **1a** is nearly planar, as indicated by the key torsion angles (Table 2). The maximum deviations from the mean plane through the non-H atoms are 0.024(1) Å for atom C(5) and 0.029(1) Å for atom

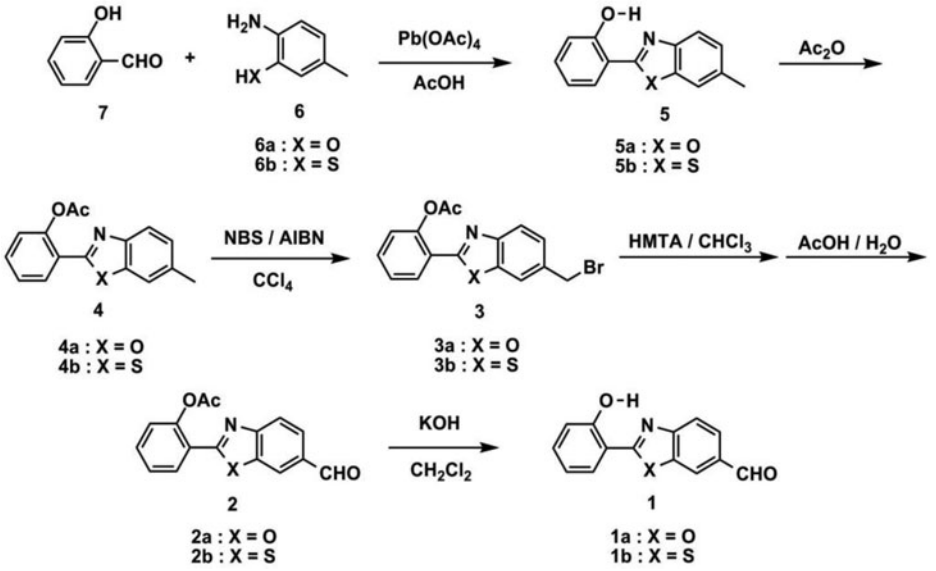

Scheme 1. The synthetic route and the chemical structures for 1a and 1b.

C(14). The dihedral angle between the mean plane of the phenol ring and the mean plane of the benzoxazol ring is 1.4(2)°, which is slightly larger than that in **1b** (3.5(2)°). Compound **1a** possesses an intramolecular O–H···N hydrogen bond, which generates an S(6) ring motif. The dihedral angle between the mean plane of the S(6) ring and the mean plane of the oxazol ring is 0.8(2)°. This, together with 2.671(2) Å of O(2)···N distance and 151(2)° of O(2)–H(2A)–N, strongly supports the S(6) ring formation. In good agreement with this observation, the ^{1}H NMR spectrum (in $CDCl_3$) revealed a significantly downfield hydroxyl signal at 11.18 ppm. The parameters of the hydrogen bond of **1a** (Table 3) are slightly different from those of **1b** (2.623(2) Å of O(2)···N distance and 150(2)° of O(2)–H(2A)–N). Additionally, there is a weak intramolecular C–H···O hydrogen bond in **1a** (2.825(2) Å of C(5)···O(1) distance and 100° of

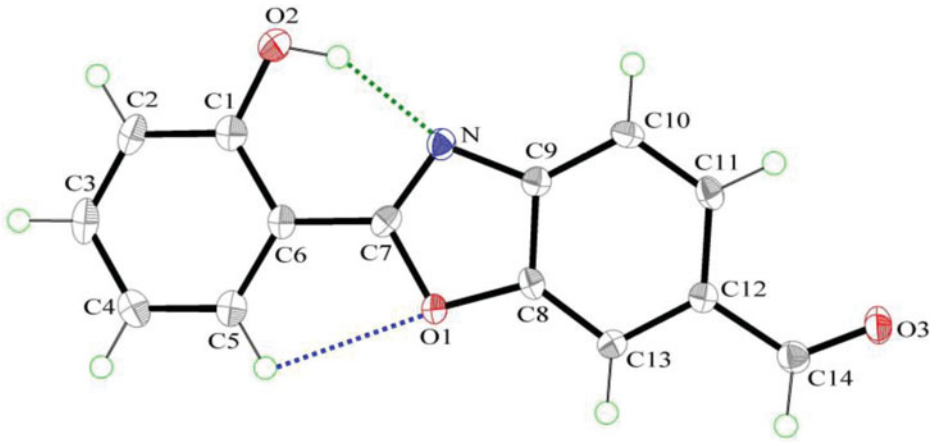

Figure 2. The molecular structure of **1a**, showing the atom-labeling scheme. Displacement ellipsoids are drawn at the 50% probability level. Blue and green dashed lines denote the intramolecular C–H···O and O–H···N hydrogen bonds.

Table 1. Crystallographic data for compounds **1a** and **1b**.

Compound	**1a**	**1b**
Chemical formula	$C_{14}H_9NO_3$	$C_{14}H_9NO_2S$
Formula weight	239.22	255.28
Crystal system	Monoclinic	Monoclinic
Space group	$P2_1/c$	$P2_1/c$
a (Å)	7.4609(5)	8.2645(3)
b (Å)	12.4804(8)	5.6449(2)
c (Å)	11.4804(6)	23.8341(9)
α (°)	90	90
β (°)	94.037(5)	98.147(2)
γ (°)	90	90
Volume ($Å^3$)	1066.34(11)	1100.69(7)
Z	4	4
D_{calc} (g cm^{-3})	1.490	1.541
μ (mm^{-1})	0.106	0.285
F_{000}	496	528
Crystal size (mm^3)	`0.58 × 0.10 × 0.08	0.38 × 0.14 × 0.04
θ range (°)	3.19–29.18	1.73–25.02
Index ranges	–10 ≦ h≦ 9	–9 ≦ h ≦ 9
–15 ≦ k ≦ 14	– 6 ≦ k ≦ 3	
–14 ≦ l ≦ 8	–28 ≦ l ≦ 28	
Reflections collected	4643	8427
Independent reflections (R_{int})	2430 (0.0341)	1943 (0.0417)
Refinement method on F^2	Full-matrix least-squares	Full-matrix least-squares
GOF on F^2	1.000	0.895
R_1 [I > 2σ (I)]	0.0548	0.0291
wR_2 [I > 2σ (I)]	0.1012	0.0558
R_1 (all data)	0.0916	0.0454
wR_2 (all data)	0.1152	0.0575
Residual (e $Å^{-3}$)	0.242 and –0.262	0.223 and –0.265

Table 2. Comparison of the experimental and optimized geometric parameters of **1a** (Å and °).

	X-ray	DFT
Bond lengths (Å)		
O(1)-C(7)	1.372(2)	1.371
O(1)-C(8)	1.387(2)	1.376
O(2)-C(1)	1.353(2)	1.344
O(3)-C(14)	1.215(2)	1.216
N-C(7)	1.305(2)	1.313
N-C(9)	1.396(2)	1.387
C(4)-C(5)	1.376(3)	1.384
C(6)-C(7)	1.449(3)	1.444
C(8)-C(9)	1.384(3)	1.403
C(12)-C(14)	1.466(3)	1.478
Bond angles (°)		
C(7)-O(1)-C(8)	103.70(15)	104.58
C(7)-N-C(9)	104.55(16)	105.31
O(2)-C(1)-C(2)	117.96(19)	117.77
C(1)-C(6)-C(7)	119.23(18)	119.20
C(8)-C(9)-C(10)	120.29(18)	120.08
O(3)-C(14)-C(12)	124.87(19)	124.78
Torsion angles (°)		
C(8)-O(1)-C(7)-N	0.00(18)	0.009
C(7)-O(1)-C(8)-C(13)	–179.69(16)	– 179.99
O(2)-C(1)-C(6)-C(7)	–0.5(2)	– 0.02
C(5)-C(6)-C(7)-O(1)	0.5(2)	0.007

Table 3. Hydrogen-bond geometry (Å, °).

D–H···Cg	d(D–H)	d(H···Cg)	d(D···Cg)	∠DHCg
O(2)–H(2A)···N	0.89(2)	1.86(2)	2.671(2)	151(2)
C(5)–H(5A)···O(1)	0.95	2.50	2.825(2)	100
C(10)–H(10A)···O(2)[a]	0.95	2.53	3.441(2)	162
C(11)–H(11A)···O(3)[b]	0.95	2.58	3.251(2)	128
C(13)–H(13A)···O(3)[c]	0.95	2.37	3.182(2)	143

Symmetry codes: (a) x, –y–1/2, z–1/2; (b) –x+1, –y, –z–1; (c) x, –y+1/2, z+1/2.

C(5)–H(5A)–O(1)), forming an S(5) motif, which may lead to an increase in the O(2)–N distance as compared to that of compound **1b** (see above). The bond-length and angle patterns of **1a** are typical, and the values of geometrical parameters are very close to those determined for **1b**.

Figure 3 shows the molecular packing of **1a** in the crystal unit cell. The crystal structure is stabilized by intermolecular π–π interactions, which links a pair of molecules into a cyclic centrosymmetric dimer. Pertinent measurements for these $\pi\cdots\pi$ interactions are: centroid–centroid distances of 3.8532(9) (red dashed lines, symmetry code: 1–X, –Y, –Z) and 3.6420(10) Å (blue dashed line, symmetry code: 1–X, –Y, –Z). The crystal packing is further stabilized by three different intermolecular C–H···O hydrogen bonds (Table 3); one between the H(10A) atom and the hydroxyl oxygen atom of a neighboring molecule (green dashed line in Fig. 3, symmetry code: x, –y–1/2, z–1/2), a second between the H(11A) atom and one carbonyl oxygen atom of another neighboring molecule (pink dashed line in Fig. 3, symmetry code: –x+1, –y, –z–1), and a third between the H(13A) atom and another carbonyl oxygen atom of a third neighboring molecule (cyan dashed line in Fig. 3, symmetry code: x, –y+1/2, z+1/2), respectively. As a result, the intermolecular π–π and C–H···O interactions link the molecules into a continuous three-dimensional framework.

Figure 4 shows the steady-state absorption and emission spectra of **1a** in cyclohexane. The absorption spectra are characterized by a lowest-lying band maximized at 336 nm with a molar absorptivity value of 1.6×10^4 M^{-1} cm^{-1}, which makes its assignment to the $\pi \rightarrow \pi^*$ transition unambiguous. Two higher energy absorption bands are also observed at 292 and 304 nm, respectively. As for the steady-state emission, compound **1a** exhibits a sole, anomalously long wavelength emission (515 nm) in cyclohexane. Figure 4 clearly shows a

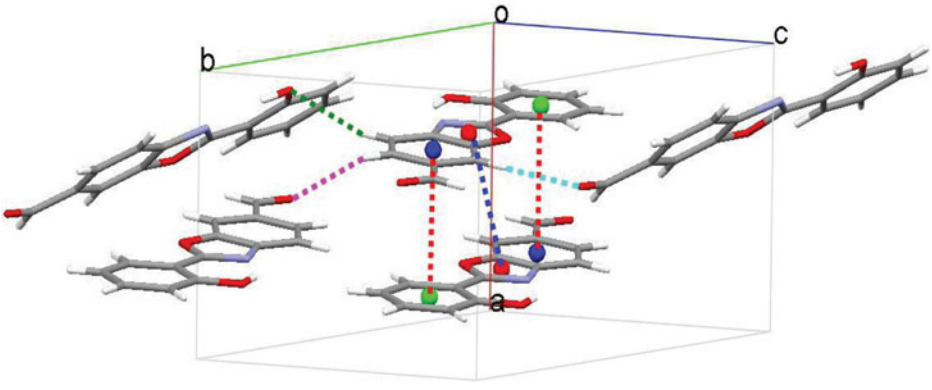

Figure 3. A packing view of **1a**. Blue and red dashed lines denote the intermolecular π–π interactions. Green, pink, and cyan dashed lines denote three different intermolecular C–H···O interactions, respectively. Cg1 (red circle), Cg2 (green circle), and Cg3 (blue circle) are the centroids of the O1/N/C7–C9, C1–C6, and C8–C13 rings, respectively.

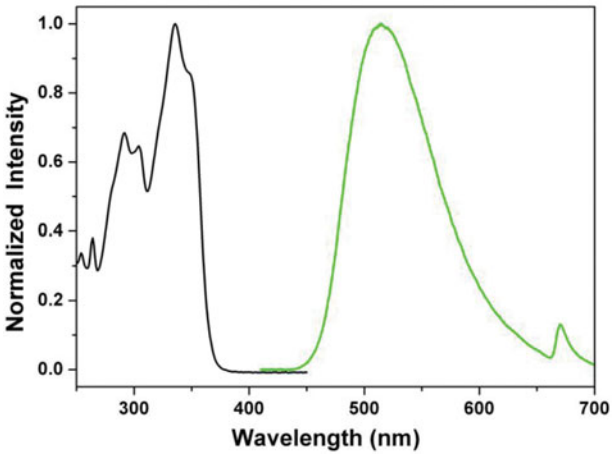

Figure 4. Normalized absorption (black line) and emission (green line) spectra of **1a** in cyclohexane.

far-separation of the energy gap between the 0-0 onset of the absorption and emission. The Stokes shift of the emission, defined by peak (absorption)-to-peak (emission) gap in terms of frequency, is determined to be as large as 10344 cm^{-1}. Accordingly, the assignment of 515 nm emission to a proton-transfer tautomer emission is unambiguous, and ESIPT takes place from the phenolic proton to the imine nitrogen, forming the keto-tautomer species.

To gain more insight into the molecular structure and electronic properties of **1a**, quantum chemical calculations were performed using density functional theory (DFT) at the B3LYP/6-31G** level. The geometric parameters (bond lengths, bond angles, and torsion angles) were compared with experimental data (Table 2). One can clearly see that there are no significant differences between the experimental and DFT/B3LYP calculated geometric parameters. Therefore, we can conclude that basis set 6-31G** is suited in its approach to the experimental results.

Figure 5 shows the HOMO and LUMO of enol and keto form of **1a**. It is apparent that the first excited states for both enol and keto forms are a dominant $\pi \rightarrow \pi^*$ transition from the HOMO to the LUMO. The HOMO of the enol-form (E) is delocalized mainly on the phenol

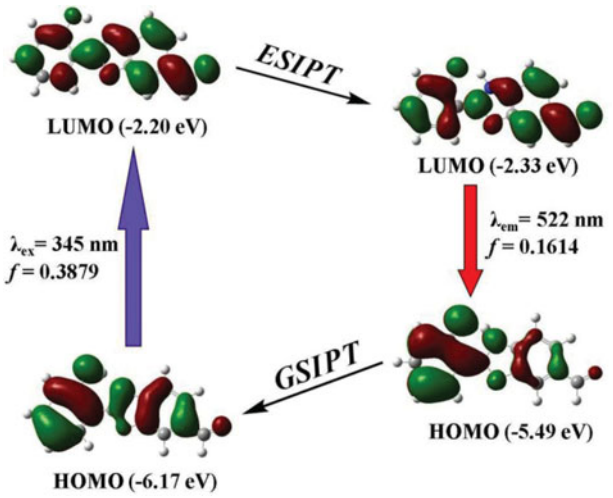

Figure 5. Selected frontier molecular orbitals involved in the excitation and emission of **1a**.

ring, while the LUMO is mostly delocalized on the benzoxazole ring, which indicates that the excitation from E to E* should involve intramolecular electron density transfer from phenol ring to benzoxazole ring. With completion of the ESIPT (GSIPT: ground-state intramolecular proton transfer) reaction, the energy level of the LUMO (HOMO) decreased from −2.20 (−5.49) to −2.33 (−6.17) eV. In addition, the absorption and emission spectra of **1a** were calculated by time-dependent DFT (TD-DFT) calculations (Franck–Condon principle). The calculated excitation (fluorescence) wavelength for the $S_0 \rightarrow S_{1-}$ ($S_1 \rightarrow S_0$) transition is 345 (522) nm, which is very close to the experimental results.

4. Conclusions

A 2-(benzo[d]oxazol-2-yl)phenol derivative, 2-(2-hydroxyphenyl)benzo[d]oxazole-6-carbaldehyde (**1a**), was synthesized and characterized by single-crystal X-ray diffraction. The crystal belongs to monoclinic, space group $P2_1/c$, with a = 7.4609(5), b = 12.4804(8), c = 11.4804(6) Å, $\alpha = 90°$, $\beta = 94.037(5)°$, $\gamma = 90°$, $V = 1066.34(11)$ Å^3, and $z = 4$. Compound **1a** possesses an intramolecular six-membered-ring hydrogen bond, from which excited-state intramolecular proton transfer takes place, resulting in a proton-transfer tautomer emission of 515 nm in cyclohexane. Furthermore, the single-crystal X-ray structure determinations described here have brought to light many interesting properties between **1a** and **1b** in the solid phase, including $\pi\cdots\pi$ stacking and intra- and intermolecular hydrogen bonding interactions. The results offer the potential to synthesize new 2-(benzo[d]oxazol-2-yl)phenol derivatives with extended molecular architectures and optical properties.

Acknowledgment

The authors appreciate the Precision Instrument Support Center of Feng Chia University for providing the fabrication and measurement facilities.

Funding

The project was supported by the Ministry of Science and Technology (MOST 104-2113-M-035-001) in Taiwan.

References

[1] Hsieh, C. C., Cheng, Y. M., Hsu, C. C., Chen, K. Y., & Chou, P. T. (2008). *J. Phys. Chem. A*, *112*, 8323.
[2] Chen, K. Y., Hsieh, C. C., Cheng, Y. M., Lai, C. H., & Chou, P. T. (2006). *Chem. Commun.*, *42*, 4395.
[3] Satam, M. A., Raut, R. K., Telore, R. D., & Sekar, N. (2013). *Dyes Pigm.*, *97*, 32.
[4] Luo, M. H., Tsai, H. Y., Lin, H. Y., Fang, S. Y., & Chen, K. Y. (2012). *Chin. Chem. Lett.*, *23*, 1279.
[5] Satam, M. A., Raut, R. K., & Sekar, N. (2013). *Dyes Pigm.*, *96*, 92.
[6] Fang, T. C., Tsai, H. Y., Luo, M. H., Chang, C. W., & Chen, K. Y. (2013). *Chin. Chem. Lett.*, *24*, 145.
[7] Chen, W. H., & Pang, Y. (2010). *Tetrahedron Lett.*, *51*, 1914.
[8] Mahapatra, A. K., Maiti, K., Sahoo, P., & Nandi, P. K. (2013). *J. Lumin.*, *143*, 349.
[9] Xie, L., et al. (2012). *Dyes Pigm.*, *92*, 1361.
[10] Maupin, C. M., et al. (2011). *J. Am. Chem. Soc.*, *133*, 6223.
[11] Lim, C. K., et al. (2011). *Dyes Pigm.*, *90*, 284.
[12] Hong, W. H., Lin, C. C., Hsieh, T. S., & Chang, C. C. (2012). *Dyes Pigm.*, *94*, 371.
[13] Huang, Q., Yang, X. F., & Li, H. (2013). *Dyes Pigm.*, *99*, 871.

[14] Prabhu, S., Saravanamoorthy, S., Ashok, M., & Velmathi, S. (2012). *J. Lumin*., *132*, 979.
[15] Patil, V. S., Padalkar, V. S., Tathe, A. B., & Sekar, N. (2013). *Dyes Pigm*., *98*, 507.
[16] Lin, W. C., Fang, S. K., Hu, J. W., Tsai, H. Y., & Chen, K. Y. (2014). *Anal. Chem*., *86*, 4648.
[17] Santos, R. C., et al. (2011). *Tetrahedron Lett*., *52*, 3048.
[18] Ito, Y., Amimoto, K., & Kawato, T. (2011). *Dyes Pigm*., *89*, 319.
[19] Ashraf, M., et al. (2012). *Dyes Pigm*., *95*, 455.
[20] Ikeda, S., et al. (2010). *J. Org. Chem*., *75*, 8637.
[21] Li, Y., et al. (2012). *J. Lumin*., *132*, 1010.
[22] Chuang, W. T., et al. (2011). *J. Org. Chem*., *76*, 8189.
[23] Xu, H., et al. (2012). *J. Lumin*., *132*, 919.
[24] Tang, K. C., et al. (2011). *J. Am. Chem. Soc*., *133*, 17738.
[25] Fang, S. K., Tsai, H. Y., Hu, J. W., & Chen, K. Y. (2014). *Int. J. Photoenergy, 2014*, Article ID 124753, 9 pages. doi:10.1155/2014/124753.
[26] Sheldrick, G. M. (1997). *SHELXS97, A Program for Automatic Solution of Crystal Structure*, University of Göttingen: Germany.
[27] Sheldrick, G. M. (1997). *SHELX97, A Program for Crystal Structure Refinement*, University of Göttingen: Germany.
[28] Frisch, M. J., et al. (2003). *Gaussian 03*, Gaussian, Inc.: Pittsburgh, PA.
[29] Chen, K. Y., Fang, T. C., Chang, M. J., Tsai, H. Y., & Luo, M. H. (2011). *Acta Cryst*., *E67*, o2862.